20
Parallel Magnetic Resonance Imaging Acquisition and Reconstruction: Application to Functional and Spectroscopic Imaging in Human Brain

Fa-Hsuan Lin and Shang-Yueh Tsai

INTRODUCTION

Magnetic resonance imaging (MRI) has contributed significantly to modern cancer diagnosis and treatment planning because of its noninvasive nature, versatile image contrast, and high spatiotemporal resolution. For decades, the quest for higher sensitivity and greater spatial and/or temporal resolution has been approached by means of increasing major field strengths, enhancing gradient performance, and improving radio frequency (RF) technology. In this chapter, we present recent MRI advances that use an RF coil array to achieve "parallel" data acquisition for higher spatiotemporal resolution.

In the context of cancer imaging, parallel MRI has immediate potential application to two long-standing challenges. First, in interventional MRI increased performance of real-time imaging is generally dependent on high spatiotemporal resolution. Second, magnetic resonance spectroscopic imaging (MRSI) has been widely utilized for diagnosis and quantification of cancer. However, given that 2D or 3D imaging of MRS data has been hampered by lengthy data encoding time, it has been rendered less clinically feasible. With the aid of parallel MRI, the challenges of achieving high spatiotemporal resolution and data encoding time can be mitigated.

In the following sections, we will present the theory of parallel MRI data acquisition and associated reconstruction algorithms, followed by examples of applications of parallel MRI for functional MRI and MRS. Although we focus on the applications of parallel MRI for brain imaging, the general concept of parallel MRI can be adaptively extended to other organs and systems with appropriate modifications to the data acquisition system and image reconstruction algorithm.

PRINCIPLES OF PARALLEL MRI

Parallel MRI is a recent advance in MRI technology that utilizes simultaneous data acquisitions from multiple RF coil receivers to improve the spatiotemporal resolution of imaging. The advantage of high signal-to-noise ratio (SNR) in phased array (Roemer et al. 1990), along with reduced k-space sampling schemes (Carlson and Minemura 1993) forms the core of parallel MRI. The idea of utilizing spatially varying sensitivity from different channels of

an RF array to reduce imaging encoding time was initially implemented in different imaging approaches (Hutchinson and Raff 1988; Carlson and Minemura 1993; Ra and Rim 1993). Currently, there exist two major commercially available implementations of parallel MRI: the image space sensitivity encoding (SENSE) approach (Pruessmann et al. 1999), and the k-space spatial harmonics (SMASH) approach (Sodickson and Manning 1997), along with its derivative, generalized autocalibrating partial parallel acquisition (GRAPPA) (Griswold et al. 2002). Implementation of parallel MRI requires data from multiple RF coil receivers, each of which observes the spatial distribution of the imaged object's spin density modulated by the coil sensitivity profile of the individual RF coil. The reduced k-space sampling in classical Fourier imaging produces aliased images in individual receivers. Given the coil sensitivity profiles from the RF array, we can unfold these aliased images.

Parallel MRI techniques can reduce scan time and thereby improve temporal resolution. Alternatively, parallel MRI can be used to increase the spatial resolution of an image within the same amount of acquisition time (Weiger et al. 2000). Additional benefits of the parallel MRI technique include lowered susceptibility artifact due to reduced read-out duration, decreased geometrical distortion due to increased phase-encoding bandwidth (Bammer et al. 2001; Schmidt et al. 2005), and lower echo-planar imaging (EPI) acoustic noise due to reduced gradient switching (de Zwart et al. 2002c).

A major price for the above-mentioned advantages is decreased image SNR. The reduction in SNR arises from two sources: reduced number of data samples, and reconstruction instability due to correlations in spatial information, as determined by the geometrical arrangement of the array coil. The first of these disadvantages is an inevitable result of reducing the number of samples. The second disadvantage might be addressed by optimizing coil geometry (de Zwart et al. 2002a) or by improving the stability of the reconstruction algorithm (Lin et al. 2004). Increased noise originating from correlated spatial information from the array elements can be estimated from the array geometry and quantified by the geometric factor map (g-factor map) (Pruessmann et al. 1999).

In practice, parallel MRI can be divided into two parts: data acquisition and image reconstruction. In data acquisition, the goal is to optimize the k-space traversing trajectory in order to achieve desired spatiotemporal resolution. In image reconstruction, the goal is to utilize the information available in an RF array to reconstruct high spatiotemporal resolution images with minimal aliasing artifact resulting from the Nyquist sampling theorem.

PARALLEL MRI ACQUISITIONS

The time required to traverse the k-space is closely related to total data acquisition time in traditional MRI. The purpose of parallel MRI is to avoid "full" sampling of the k-space by skipping certain data collection points. The skipped k-space data produce aliased images, as predicted by the Nyquist sampling theorem. Using information from all channels in the RF coil array, the skipped data can be numerically interpolated from sampled data to restore full field-of-view (FOV) images without aliasing artifacts. Typically, in rectilinear Cartesian

coordinates, parallel MRI skips data in the phase-encoding direction; skipping data in the frequency-encoding direction saves little data acquisition time because the duration of the frequency-encoding gradient is the same regardless of whether sampling is full or skipped. Parallel MRI acquisition with skipped phase encoding data can reduce data acquisition time and thus improve temporal resolution. The benefit of skipping data collection in the phase encoding direction can also be translated to higher bandwidth and less geometrical distortion (Bammer et al. 2001; Schmidt et al. 2005).

In rectilinear Cartesian coordinates, implementing parallel MRI acquisition can be easily achieved by increasing the step size in the phase-encoding direction. The EPI trajectory is therefore similar to that of segmented EPI (McKinnon 1993). Reconstruction of individual EPI segments from all array elements renders itself as parallel MRI. When using non-Cartesian sampling such as spiral imaging, parallel MRI acquisition can be implemented by reducing the number of spiral arms to cover the k-space. These 2D sampling trajectories can be extended to 3D, which has two phase-encoding directions in Cartesian sampling. Parallel MRI can reduce sampling in both phase-encoding directions by using complimentary information from array elements to reconstruct images without aliasing artifacts (Weiger et al. 2002a). Optimization of data acquisition schemes in parallel MRI can also be combined with RF modulation to control spatial aliasing in accelerated acquisition, and thereby improve reconstruction quality (Breuer et al. 2005a).

The capability for improving temporal resolution makes parallel MRI an appealing data acquisition approach. When applied to dynamic scans, where imaging planes or volumes are repeated, parallel MRI data acquisition can be further optimized by taking both k-space and time domain into consideration. For example, TSENSE (Kellman et al. 2001) utilizes interleaved segmented EPI acquisition, each segment of which can later be reconstructed from an aliased image to a full-FOV image. This approach can be further combined with a time-domain filtering method, such as UNFOLD (Madore et al. 1999), to further improve the temporal resolution of dynamic scanning (Tsao et al. 2003). Similar to TSENSE, which uses SENSE as the reconstruction kernel, the same time-interleaved k-space sampling was used in the implementation of TGRAPPA, which uses GRAPPA as the reconstruction kernel (Breuer et al. 2005b).

In parallel MRI, sensitivity maps for all channels in the coil array critically determine the quality of the reconstructed image. Traditionally, a separate scan is required to estimate coil maps (Pruessmann et al. 1999). Because coil maps vary smoothly over the FOV in most cases, low spatial resolution scans usually are adequate to serve this purpose. Low spatial resolution in coil sensitivity maps inspired the integration of data collection for coil map estimation into the accelerated parallel MRI acquisition; accelerated scanning is achieved by skipping data with high spatial frequency while at the same time maintaining full sampling around the center of the k-space for coil map estimation. This method is called “auto-calibration” because in single acquisition such data potentially contain both coil map information and the image to be reconstructed. And it was used in SMASH (Jakob et al. 1998),

SENSE (Madore 2004), and GRAPPA implementations (Griswold et al. 2002). Different from rectilinear Cartesian trajectory sampling, non-Cartesian sampling using a spiral trajectory is intrinsically self-calibrated. This means that the dense sampling around the center of k-space in spiral trajectory can be used as the coil sensitivity maps required in parallel MRI reconstruction. Methods have been proposed to utilize the more densely sampled central part of the k-space to extract coil maps for improved reconstructions (Yeh et al. 2005a; Heberlein and Hu 2006).

PARALLEL MRI RECONSTRUCTIONS

The goal of reconstructing parallel MRI data is to remove aliasing artifacts using coil sensitivity information and observations from multiple channels in a coil array. Currently, there are two prevailing major variants of reconstruction algorithms: the k-space-based SMASH/GRAPPA method (Sodickson and Manning 1997; Griswold et al. 2002) and the image domain SENSE method (Pruessmann et al. 1999). In practice, image reconstruction can be divided into three stages: The first stage is preparation of parallel MRI reconstruction, which includes quantification of array coil performance, coil map estimation, and preprocessing of accelerated data. The second stage is reconstruction of the full-FOV image from under-sampled k-space data. The third stage is combination of reconstructed images for final presentation.

In the first stage, it is typically desirable to quantify the correlation between channels in an RF coil array. Correlated information between array channels causes redundant observations from different channels. And it may thus degrade the quality of reconstructed image, because of insufficient independent information to remove aliasing. Correlations between channels in an array may be due to imperfection of coil fabrication, such as common mode signal or electromagnetic coupling. Typically, we can quantify the correlation among channels of an RF coil array by the noise covariance matrix, which can be estimated experimentally by turning off RF excitation while turning on data acquisition for a period of time (Pruessmann et al. 1999). The noise covariance matrix can thus be calculated using the time series from all channels, and its structure indicates the correlation between channels. Ideally, we expect minimal correlation among channels, corresponding to a noise covariance matrix with minimal off-diagonal entries. A large off-diagonal entry implies that information between two channels is highly correlated, and thus the information from these two corresponding channels may be redundant. Given a quantitative noise covariance matrix, we can "whiten" the parallel MRI acquisition to balance the independent information between channels in a coil array.

The other essential part of preparing parallel MRI data reconstruction is coil sensitivity map estimation. Using a separate sensitivity map scan, we may apply either local polynomial fitting (Pruessmann et al. 1999) or novel wavelet filtering (Lin et al. 2003) to estimate coil maps. However, estimation of coil maps can be avoided if the in vivo sensitivity method is employed (Sodickson 2000). Unlike traditional SENSE/SMASH reconstructions, the in vivo sensitivity method estimates the ratio of the spin density in the accelerated scan over that in the full-FOV reference scan. Restoration of the final

reconstructed image from the estimated full-FOV spin density ratio requires a multiplication operation. The estimated spin density ratio must multiply the coil sensitivity maps, which are full-FOV reference images themselves, to obtain coil-by-coil reconstructed images. The benefit of the in vivo sensitivity is that it requires no coil sensitivity map estimation; thus making it possible to avoid errors associated with misspecification of coil maps. However, ill conditioning at pixels, where the ratio between accelerated and unaccelerated scans is not defined, also limits the ability of the in vivo sensitivity method. Similarly, GRAPPA reconstruction (Griswold et al. 2002) also does not require explicit coil map estimation. In GRAPPA, coil map information is embedded in auto-calibration scans (ACS), which are usually k-space samples around the center of the k-space satisfying the Nyquist sampling theorem. The purpose of ACS is to sample some k-space data, which would be avoided in the accelerated scan, in order to estimate the parallel MRI reconstruction coefficients. This auto-calibration technique has also been employed in spiral trajectory MRI (Yeh et al. 2005b).

The core of parallel MRI employs undersampled data from multiple channels in an RF coil array and coil map information to restore full-FOV images. Usually, due to the computational efficiency of an analytical solution, such restoration is done by linear (weighted) least square fitting (Sodickson and Manning 1997; Pruessmann et al. 1999). Mathematically, the least square fitting solution corresponds to an optimization problem with a cost function defined as the L-2 norm of the model error, the discrepancy between actually observed accelerated data and model-predicted data, for all channels in a coil array. To further improve the stability of parallel MRI reconstructions, Tikhonov regularization framework (Tikhonov and Arsenin 1977) has recently has shown to be effective for incorporating spatial prior in the cost function to reduce noise amplification arising from the "unfolding" process of aliased matrix (Lin et al. 2004). Given appropriate regularization parameters, prior regularized parallel MRI reconstructions show improved stability in both structural and functional MRI (Lin et al. 2004, 2005).

Typically with Cartesian sampling, parallel MRI data reconstruction can be separated into many small linear systems, each of which consists of aliasing pixels in the final reconstructed image. Such reconstruction is possible because the point-spread function derived from the k-space sampling pattern separates the reconstruction into many decoupled linear systems. However, for non-Cartesian sampling methods, such as spiral imaging, we cannot separate reconstruction into many smaller linear systems. Instead, we must directly solve a huge linear equation of size n^2-by- n^2, where n^2 is the number of voxels in the whole 2D image. An iterative solver using a Conjugated-Gradient (CG) algorithm has been proposed to address this issue (Pruessmann et al. 2001).

Finally, reconstruction of parallel MRI may involve strategies to combine the estimated spin distribution from all channels in the array. Using SENSE reconstruction, this process is implicitly implemented during image reconstruction using coil sensitivity as the weighting function to produce a final composite image. In SMASH/GRAPPA imaging, alternatives to combining different channels in the array after parallel MRI reconstruction have been proposed, including direct averaging,

matched filter combination, and sum-of-squares combination (McKenzie et al. 2001; Griswold et al. 2002).

MATHEMATICAL FORMULATION

Formation of aliased images from multiple receivers in parallel MRI can be formulated as a linear operation to "fold" the full-FOV spin density images (Sodickson and McKenzie 2001).

$$\vec{y} = A\vec{x} \tag{20.1}$$

Here $\vec{y}$ is the vector formed from the pixel intensities recorded by each receiver (folded image) and $\vec{x}$ is the vector formed from the full FOV image. The encoding matrix A consists of the product of the aliasing operation due to k-space data sub-sampling and modulation of coil-specific sensitivity over the image. The goal of image reconstruction is to solve for $\vec{x}$ given our knowledge of A derived from understanding the folding process and an estimate of the coil sensitivity maps. Whereas Eq. 20.1 is expressed in the image domain SENSE approach (Pruessmann et al. 1999), similar linear relationships are formed in the k-space-based SMASH (Sodickson and Manning 1997) method. Furthermore, the same basic formulation is used in either the in vivo sensitivity method (Sodickson 2000), or the conventional SENSE/SMASH methods requiring coil sensitivity estimation. In general, Eq. 20.1 is an over-determined linear system, i.e., the number of array coils, which is the row dimension of $\vec{y}$, exceeds the number of pixels that folds into the measured pixel; the row dimension of $\vec{x}$.

To solve for $\vec{x}$ (the full FOV image), the over-determined matrix is inverted utilizing least-square estimation (Pruessmann et al. 1999).

$$\begin{aligned} \vec{x} &= U\vec{y} \\ &= \left(A^H \Psi^{-1} A\right)^{-1} A^H \Psi^{-1} \vec{y} \end{aligned} \tag{20.2}$$

where the H superscript denotes the transposed complex conjugate and Ψ is the receiver noise covariance (Pruessmann et al. 1999). When Ψ is positive semi-definite, the eigen decomposition of the receiver noise covariance (Λ and V) leads to the unfolding matrix, U, using the whitened aliasing operator $\tilde{A}$ and the whitened observation $\tilde{y}$. Whitening of the aliasing operator will be used in the regularization formulation introduced in the next section.

$$\begin{aligned} \Psi &= V\Lambda V^H \\ \tilde{A} &\equiv \Lambda^{-1/2} V^H A \\ \tilde{y} &\equiv \Lambda^{-1/2} V^H \vec{y} \\ \vec{x} &= U\tilde{y} \\ &= (\tilde{A}^H \tilde{A})^{-1} \tilde{A}^H \tilde{y} \end{aligned} \tag{20.3}$$

Whitening incorporates the receiver noise covariance matrix implicitly allowing optimal SNR reconstruction within the regularization formulation. The noise sensitivity of the parallel imaging reconstruction is thus quantified by amplification of the noise power that results from the array geometry. This g-factor is thus written (Pruessmann et al. 1999)

$$\begin{aligned} g_{\rho\rho} &= \frac{\sqrt{X_{\rho\rho}^{parallelimaging}}}{\sqrt{R}\sqrt{X_{\rho\rho}^{full}}} \\ &= \sqrt{[(\tilde{A}^H \tilde{A})^{-1}]_{\rho\rho} (\tilde{A}^H \tilde{A})_{\rho\rho}} \end{aligned} \tag{20.4}$$

The subscript ρ indicates the voxels to be "unfolded" in the full FOV image, and $\boldsymbol{X}$ denotes the covariance of the reconstruction image vector $\vec{x}$. Here R denotes the factor by which the number of samples is reduced (the acceleration rate).

Tikhonov regularization (Tikhonov and Arsenin 1977) provides a framework to stabilize the solution of an ill-conditioned linear equation. Using Tikhonov regularization, the solution of Eq. 20.1 can be written as

$$\vec{x}^{\lambda} = \arg\min_{\vec{x}} \left\{ \left\| \tilde{A}\vec{x} - \tilde{y} \right\|_2 + \lambda^2 \left\| L(\vec{x} - \vec{x}^0) \right\|_2 \right\} \tag{20.5}$$

Here λ^2 is the regularization parameter. L is a positive semi-definite linear transformation, $\vec{x}^0$ denotes the prior information about the solution $\vec{x}$, and $\|\bullet\|_2$ represents the L-2 norm. The second term in Eq. 20.5, defined as the prior error, is the deviation of the solution image from the prior knowledge. The first term, defined as the model error, represents the deviation of the observed aliased image from the model observation, which is a folded version solution image. The regularization parameter determines the relative weights with which these two estimates of error combine to form a cost function.

Consider the extreme case when λ^2 is zero and we attempt to minimize only the first term – a calculation that is equivalent to solving the original equation, $\vec{y} = A\vec{x}$, without conditioning (conventional SENSE reconstruction). On the other extreme, when λ^2 is large, the solution will duplicate of the prior information $\vec{x}^0$. Thus, the regularization parameter λ^2 quantifies the trade-off between model error and prior error. An appropriate chosen λ^2 (regularization) decreases the otherwise complete dependency on the whitened model ($\tilde{A}$) and the whitened observation ($\tilde{y}$), to constrain the solution to within a reasonable "distance" from the prior knowledge ($\vec{x}^0$). Thus regularization increases the influence of prior knowledge full FOV image information during parallel MRI reconstruction.

Given the regularization parameter λ^2 and defining L as an identity matrix, the solution of Eq. 20.4 is written (Hansen 1998):

$$\begin{aligned} \vec{x}^{\lambda} &= \sum_{j=1}^{n} \left(f_j \frac{\vec{u}_j^{\mathrm{H}} \tilde{y}}{s_{jj}} + (1 - f_j) \vec{\upsilon}_j^{\mathrm{H}} \vec{x}^0 \right) \vec{\upsilon}_j \\ f_j &= \frac{s_{jj}^2}{s_{jj}^2 + \lambda^2} \cong \begin{cases} 1, S_{jj} >> \lambda \\ s_{jj}^2 / \lambda^2, S_{jj} << \lambda \end{cases} \end{aligned} \tag{20.6}$$

Here $\vec{u}_j$, $\vec{\upsilon}_j$, and s_{jj} are the left singular vector, right singular vector and singular value of $\tilde{A}$, respectively, generated by singular value decomposition (SVD); singular values and vectors are indexed by j. This calculation leads to the following matrix representations:

$$\begin{aligned} \vec{x}^{\lambda} &= V\Gamma U^H \tilde{y} + V\Phi V^H \vec{x}^0 \\ VAR(\vec{x}^{\lambda}) &= V\Gamma^2 V^H \\ \Gamma_{ii} &= \frac{f_i}{s_{ii}} = \frac{s_{ii}}{s_{ii}^2 + \lambda^2} \\ \Phi_{ii} &= 1 - f_i = \frac{\lambda^2}{s_{ii}^2 + \lambda^2} \end{aligned} \tag{20.7}$$

Using regularization and Eq. 20.4, the ratio of the noise levels between the regularized parallel MRI reconstruction and the original full FOV image normalized by the factor of acceleration yields the local geometry factor for noise amplification.

$$g_{\rho\rho} = \sqrt{[(V\Gamma^2 V^H)]_{\rho\rho}[(VS^2 V^H)]_{\rho\rho}} \quad (20.8)$$

Inside the square root of Eq. 20.8, the first square bracket term denotes the variance of unfolding using regularization from Eq. 20.7; the second square bracket term denotes the variance of the full FOV reference image.

APPLICATION – SENSE HUMAN BRAIN FUNCTIONAL MAGNETIC RESONANCE IMAGING

Applications of parallel MRI acquisition protocols for fMRI experiments have been reported by different groups, which used either the PRESTO sequence (Golay et al. 2000) or the gradient-echo EPI sequence (de Zwart et al. 2002b; Weiger et al. 2002b; Preibisch et al. 2003). The rationale for using parallel MRI is that fMRI data acquisition protocol focuses on enhancement of spatiotemporal resolution due to reduced k-space traversing time. At high field (≥3T) scanners, T2* relaxation time of human gray matter may be less than 30 ms in areas that exhibit pronounced field inhomogeneities (Barth et al. 1999). Traditionally such a short T2* made single-shot EPI intractable for sufficient spatiotemporal resolution because the data acquisition time was insufficient to traverse the entire k-space. With parallel imaging, the time needed to traverse the k-space is reduced by means of mathematically "unfolding" the aliased images from individual receivers in the array. Reduced k-space traversing time also benefits the reduction of susceptibility artifacts and geometrical distortion originating from local magnetic field inhomogeneity. This is because the shortened readout time for data acquisition contributes to reduced local spin dephasing within individual voxels and produces higher bandwidth in the phase-encoding direction. Another significance of utilizing SENSE as the fMRI data acquisition protocol at high fields includes lowered acoustic noise owing to gradient switching for complete k-space trajectory traversing (de Zwart et al. 2002c).

Echo-planar imaging (EPI) is the most popular functional MRI acquisition protocol for capturing T2*-weighted image contrast derived from intrinsic hemoglobin, which can infer local neural activity. Here we demonstrate the effect of reduced EPI distortion with GRAPPA-reconstructed EPI on a 3T scanner (Siemens Medical Solution, Erlangen, Germany) equipped with an eight-channel head phased array coil (Figure 20.1). The imaging parameters are: FOV = 200 mm, TR/TE = 2,000/30 ms, Flip angle = 90°, slice thickness = 3 mm, bandwidth = 1,440 Hz. Note that image distortion around the frontal and temporal lobes was improved using GRAPPA imaging. Regularization can also suppress noise at the center of the reconstructed image, compared to unregularized reconstruction in the same acceleration rate.

To further demonstrate how EPI with reguarlized parallel MRI reconstruction can be applied to human brain fMRI experiments, we collected a set of blocked-design visual fMRI data from a 3T scanner equipped with an eight-channel phased array coil. And subsequently SENSE reconstructions were performed. We recruited one healthy subject for the study after receiving approval from the Institutional Review Board and obtaining the subject's

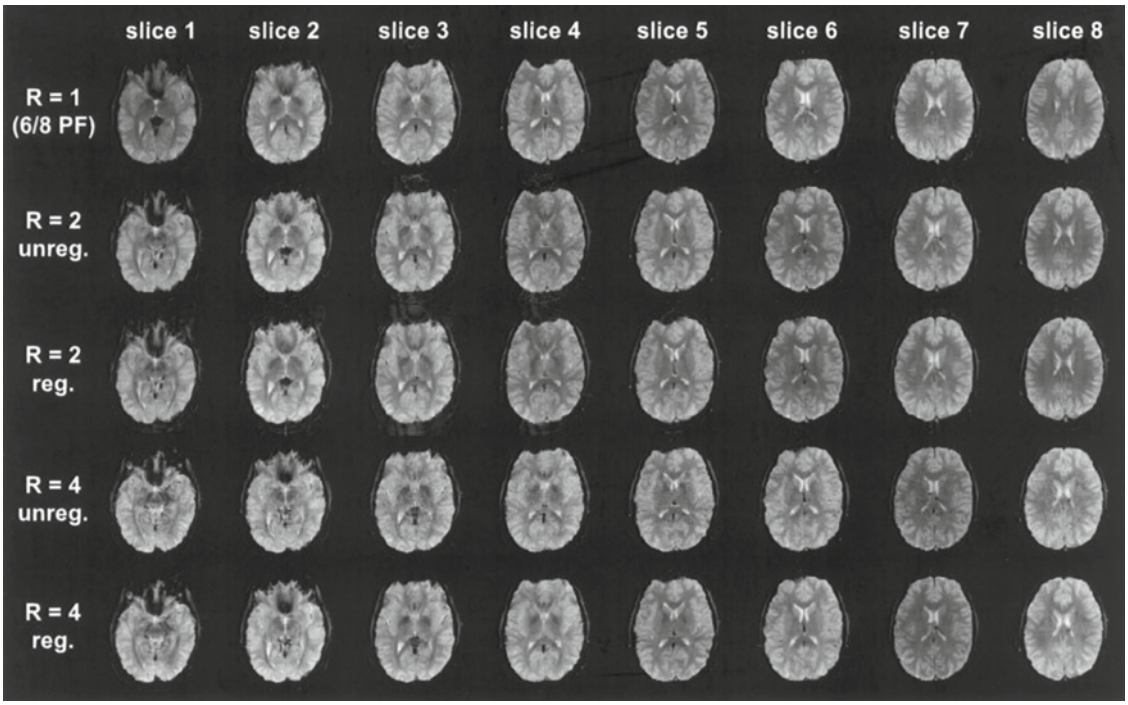

FIGURE 20.1. Compared to non-accelerated reconstruction (R = 1) with 6/8 partial Fourier (PF) sampling, GRAPPA EPI reconstructions at 2X (R = 2) and 4X (R = 4) accelerations show decreased distortion around the temporal and frontal lobes, where susceptibility and B_0 inhomogeneity is strong. At the same acceleration rate, regularized (reg.) reconstructions show less noise amplification than unregularized (unreg.) reconstructions, particularly around the center of the brain

informed consent. A checkerboard visual stimulus, designed to display either continuous flashing checkerboards at 4 Hz (the "on" condition), or fixation (the "off" condition), was presented to the subject. Three "off" conditions and two "on" conditions of seconds each were alternately presented, starting with the "off" condition. We used a 2D EPI sequence with the parameters: TR = 2,000 ms, TE = 50 ms, flip angle = 90°, slice thickness = 5 mm with 0.5 mm gap, 14 slices, FOV = 200 × 200 mm, image matrix = 128 × 128 for image acquisition. We collected three-segment EPI data (20 volumes in composition reconstruction, with eight "on" and 12 "off" conditions; ten dummy scans) and four-segment EPI data (15 volumes in composition reconstruction with six "on" and nine "off" conditions; ten dummy scans). Phase encoding was in the anterior-posterior direction. We used the in vivo sensitivity method to reconstruct accelerated images and thus avoid misestimating the coil sensitivity maps. We also acquired the full FOV spatial prior required for regularized reconstruction by temporal collapsing EPI segments using interleaved segmented EPI (Lin et al. 2005). Figure 20.2a shows the *t* statistics maps of the 3T visual fMRI experiment using SENSE EPI both with and without regularization at three- and four-fold accelerations. At three-fold SENSE acceleration,

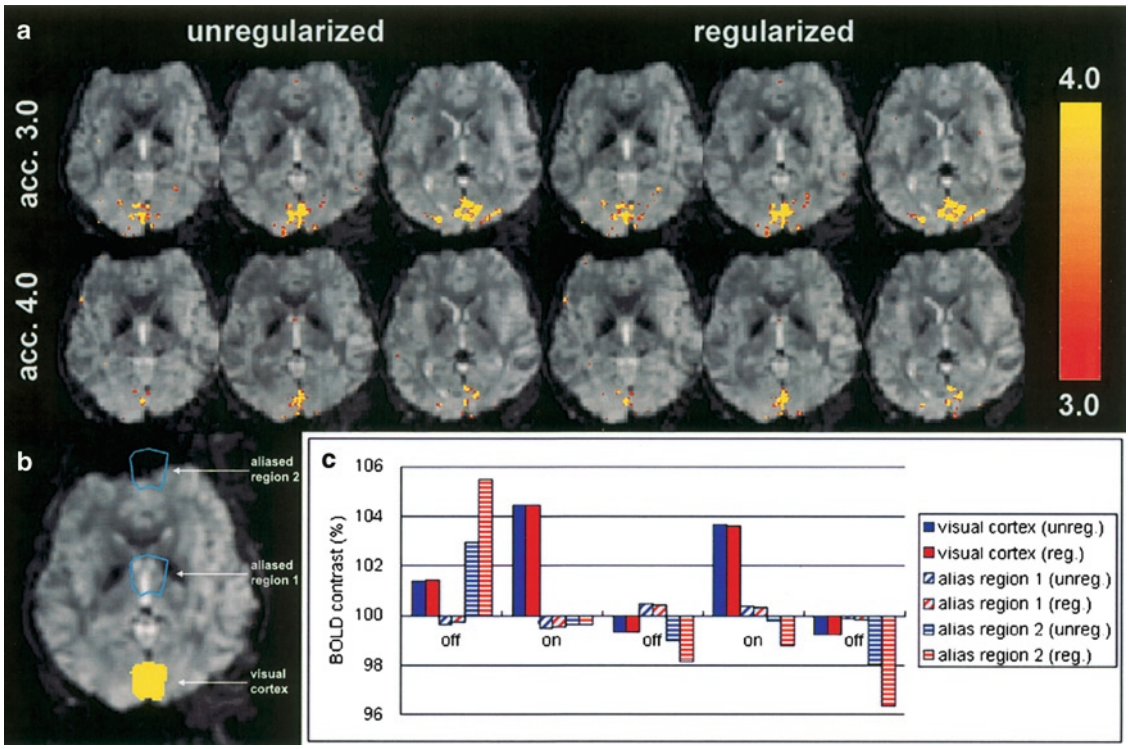

FIGURE 20.2. (**a**) The *t* statistics maps calculated from 3X and 4X SENSE reconstructions. (**b**) EPI image depicting the three aliased regions with 3X acceleration. One of the aliased regions, highlighted in yellow, is the visual cortex. (**c**) The time courses of the three aliased regions. Note that only the time course from the visual cortex corresponded well to the stimulus paradigm

regularized reconstructions yielded larger activated functional areas than unregularized reconstructions around the occipital lobe (regularized: 2,327 mm^2; unregularized: 2,139 mm^2). A similar increase in sensitivity by regularization was also observed in the four-fold SENSE acceleration (regularized: 896 mm^2; unregularized: 735 mm^2).

Figure 20.2b shows the three regions aliased with three-fold acceleration. One of the aliased regions shown here is visual cortex region, highlighted in yellow. The corresponding time courses of all three aliased regions are depicted in Figure 20.2c. Note that only the activated visual cortex region exhibited a time course that matched to the stimulus paradigm. The other two aliased regions showed either low BOLD contrasts in all conditions or a time course mismatched to the stimulus paradigm. We have previously reported more detailed Monte Carlo simulations on the improvement of the stability of SENSE EPI reconstructions (Lin et al. 2005).

Here we demonstrated the benefits of parallel MRI to reduce distortion artifact. Spatial prior can also be incorporated to regularize reconstructions for suppression of noise levels introduced in parallel MRI reconstructions during dynamic fMRI scan. Further improvement of parallel MRI reconstruction can potentially be accomplished by using a large-*N* coil array and optimizing the k-space trajectory for accelerated scans.

APPLICATION – SENSE PROTON SPECTROSCOPIC IMAGING

In vivo magnetic resonance spectroscopy (MRS) and magnetic resonance spectroscopic imaging (MRSI) have been used for almost 3 decades to measure possible prognostic or diagnostic markers in living tissue (Gillies and Morse 2005). The former has been suggested as a clinical tool for cancer in various regions of the body (Bellouche-Babari et al. 2005) and is a primary focus for applications in brain cancer (Preul et al. 1996). The major goals of MRS studies for applications in cancer diagnosis and treatment planning are to identify types and grades of cerebral neoplasm (Del Sole et al. 2001). Because MRS is sensitive to alterations in the chemical signals of various metabolites including choline (Cho), creatine (Cr), lactate, myoinositol, and N-acetyl-aspartate (NAA), MRS technology can help clinicians evaluate brain tumors and neoplasm metabolic states. The most frequently observed biomarkers of brain tumors include decreases in choline and lactate and increases in NAA. Magnetic resonance spectroscopic imaging (MRSI) techniques allow metabolic "images" to be obtained throughout the volume of interest with a single measurement (Brown et al. 1982), but are often limited by long echo times to reduce contamination from overwhelming peripheral lipids. Short-TE MRSI techniques are feasible and allow additional measurements of lipid signals in brain tumors. Measuring these signals is significant because their levels are indicative of macrophage activity in necrosis. Although identification of a tumor mass and assessment of its size and vasculature are best achieved with MRI, MRSI can provide additional biochemical information that can be crucial for tumor classification, differential diagnosis and follow-up (Preul et al. 1998). The ability to display the metabolite distribution as a map is therefore very important and useful in clinical settings (Preul et al. 1998).

Magnetic resonance spectroscopic imaging (MRSI) measures spatially encoded time-domain signals from free-induction decay (FID), stimulated echoes, or spin echoes using gradient phase encoding to resolve the two- or three-dimensional spatial distribution of spectroscopic information that originated from different locations within the field-of-view (FOV). Data acquisition time grows in proportion to the spatial encoding specified in the imaging protocol. For example, in 2D proton MRSI with 32×32 imaging matrix and TR = 2 s, encoding time is >30 min.

Several methods have been proposed to speed up conventional MRSI: Reduced k-space encoding techniques such as circular k-space sampling (Maudsley et al. 1994), variable repetition times for different phase encoding steps (Kuhn et al. 1996), and individually phase-encoded multi-echo techniques (Duyn et al. 1993) offer moderate acceleration of conventional phase encoding. Implementation of echo-time-encoded high-speed imaging methods is straightforward (Haase 1990), but achieving high spectral resolution at large spectral width is still time-consuming. Furthermore, short echo times are not feasible, and sensitivity is usually lower than with conventional techniques (Pohmann et al. 1997).

Even with above-mentioned efforts to accelerate MRSI, three-dimensional spatial encoding is still not clinically feasible. Data quality during such long data acquisition

times can be seriously degraded by head motion and scanner instability. Motion artifact is especially problematic with respect to tremors associated with neural degenerative diseases such as Alzheimer's, and dynamic metabolic imaging, which requires repeated measurements to provide time-resolved information, is limited to rather coarse temporal resolution.

Much faster spatial-spectral encoding can be achieved using either echo-planar (Posse et al. 1994) or spiral read-out methods (Adalsteinsson et al. 1998). Using echo-planar readout, proton-echo-planar-spectroscopic-imaging (Pepsi) can accelerate encoding times in human brain by more than an order of magnitude and has been developed for clinical MR scanners to measure two-dimensional metabolite distributions at short TE in just 1 min (minimum acquisition time for a 32 × 32 matrix is 64 s with TR = 2 s) (Posse et al. 1995), and three-dimensional metabolite distributions in just a few minutes (Posse et al. 1994). Proton-echo-planar-spectroscopic-imaging (PEPSI) has also been employed for time-resolved metabolic imaging to map dynamically changing lactate concentrations during respiratory and metabolic challenges (Posse et al. 1997) and to characterize metabolic dysfunction during sodium-lactate infusion in patients with panic disorder (Dager et al. 1999).

Here we present the combination of PEPSI and parallel MRI, specifically SENSE reconstruction, to further accelerate data acquisition in high-speed spectroscopic imaging. The major motivation of this approach is to tradeoff SNR for rapid spatial encoding and reduced motion sensitivity during long data acquisition times. In vivo human subject experiments were performed under the supervision of the Institutional Review Board, and with subjects' informed consent. PEPSI (Posse et al. 1995) was performed on healthy volunteers, using a 3T scanner (Trio, SIEMENS Medical Solution, Erlangen, Germany) equipped with an eight-channel surface array coil that covers the whole brain circumferentially by eight surface coils. This procedure includes water suppression by chemical shift selective saturation (CHESS) sequence (Haase et al. 1985), complete eight-slice outer volume suppression along the perimeter of the brain, spin-echo excitation, and fast spatial-spectral encoding of the half-echo using an EPI read-out gradient train along the x-axis (Posse et al. 1995). Data were acquired at 2.5 KHz per data point, using online regridding to account for ramp sampling (O'Sullivan 1985), and 1,024 gradient inversions. Reconstructed spectral width after even/odd echo editing was 1,080 Hz. Additional phase encoding along the Y-axis was applied to obtain 2D spatial encoding. SENSE for spatiotemporal acceleration, spatial phase encoding along the Y-axis was skipped by sampling one k-space line in a block of two, three, or four consecutive k-space lines in the phase encoding direction to achieve 2X, 3X, and 4X acceleration, respectively. Both non-water-suppressed (NWS) and water-suppressed (WS) PEPSI data were collected. Non-water suppressed data were collected without spatial presaturation and used for automatic phase and frequency shift correction. Proton-Echo-Planar-Spectroscopic Imaging (PEPSI) data were acquired from a para-axial slice at the upper edge of the ventricles with TR of 2 s and short TE of 15 ms using a 32 x 32 spatial matrix with FOV of 220 mm; slice thickness was 15 mm. Such data were collected with eight

averages, among which single average data were also extracted to test whether SNR was sufficient for SENSE acceleration. The acquisition times for single-average and eight-average data were 64 and 512 s, respectively, without SENSE acceleration.

Reconstructed PEPSI data with eight averages were reconstructed with LCModel fitting. Water-suppressed data were acquired with 8.5, 4.25, 2.8 and 2.1 min acquisition times for fully sampled, 2X, 3X, and 4X SENSE, respectively. The three major metabolite peaks representing Cho, Cre, and NAA were also observed in unaccelerated scans and 2X, 3X, and 4X accelerated data with similar width and shape (not shown here). The shape of the baseline in all reconstructed data was mostly similar. The Cho, Cre, and NAA metabolite maps are shown in Figure 20.3 (top panel). The maps of fully sampled and 2X SENSE accelerated data are very similar. Signal-to-noise constraints in the 3X and 4X SENSE results failed to preserve the homogenous metabolite distribution in brain parenchyma regions seen in the fully sampled data.

A single signal average was extracted from the same data set with eight averages to evaluate the effect of SNR loss on SENSE acceleration quality. The Cho, Cre, NAA metabolite maps are shown in Figure 20.3 (bottom panel). Single-average, fully sampled data generated homogeneous maps. With only slight degradation, using 2X SENSE, which corresponds to 32 s data acquisition time, the metabolite maps were still comparable to the unaccelerated maps. 3X and 4X SENSE acceleration with 22 s and 16 s data acquisition times generated more noisy metabolite maps in brain parenchyma, indicating insufficient SNR for SENSE acceleration in both cases.

We have demonstrated the feasibility of using SENSE reconstruction to accelerate high-speed gradient-encoded MRSI data acquisition, which was achieved by trading off image SNR for faster data acquisition time. The reduced SNR results from decimated data samples and reconstruction-associated noise amplification. We have shown that at high field (≥3T) the combination of PEPSI with SENSE can further reduce the intrinsic single-average 64 s data acquisition time for a 32 × 32 matrix to 32 s (2X SENSE) with little degradation of metabolite information. With even higher field strength and improved RF coil arrays, we anticipate that SENSE-accelerated metabolite mapping with scan times on the order of a few seconds will become feasible. Another appropriate application of single-average SENSE PEPSI is the context of transient high SNR, such as in hyperpolarized 13C experiments (Golman et al. 2003). At lower field (≤1.5 T), averaging was necessary to maintain SNR, and the chief advantage of the SENSE PEPSI imaging technique is thus reduced motion sensitivity associated with shortened acquisition time for a single average. Reduced motion sensitivity is particularly advantageous in clinical studies of patients with movement disorders. The overall SNR can be maintained with averaging, provided that the g-factor does not deviate too far from 1.0 using a dedicated array coil design and optimal coil placement.

Sensitivity-encoding (SENSE) acceleration is particularly important to reducing long scan times in 3D spatial encoding, which is currently under development in our laboratory. As mentioned above,

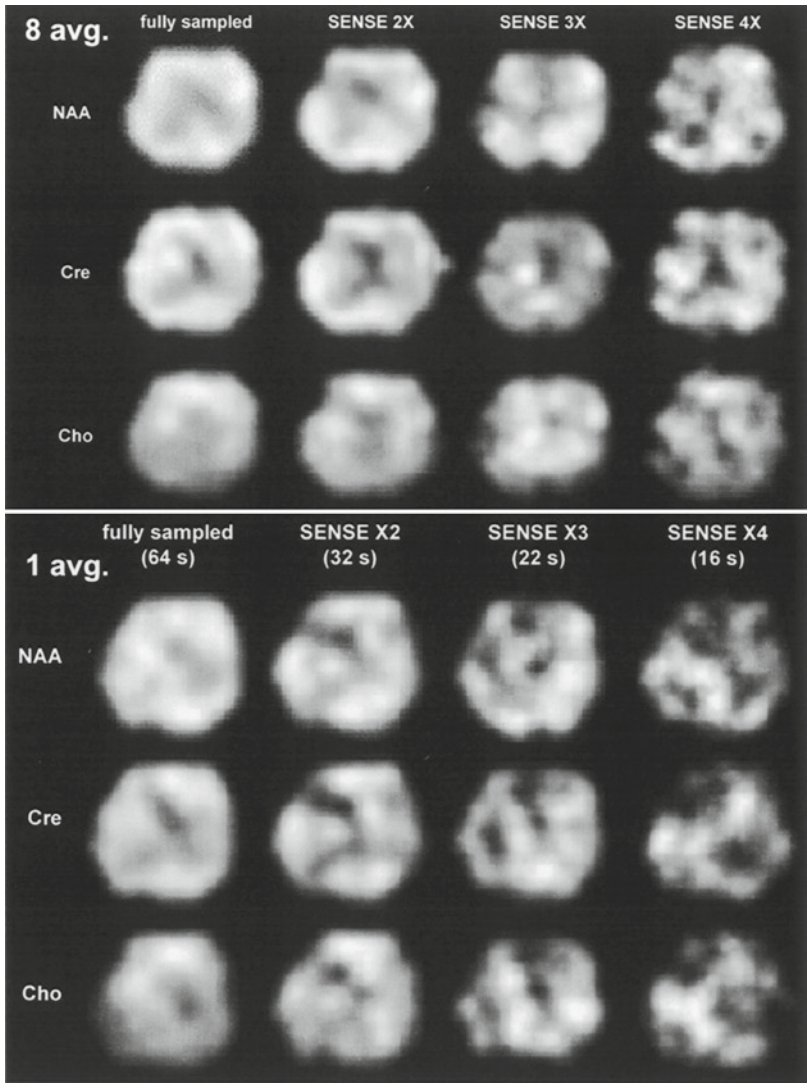

FIGURE 20.3. NAA, creatine (Cre), and choline (Cho) metabolite maps measured in a para-axial slice at the upper edge of the ventricles from full sampled data and 2X, 3X, 4X SENSE acceleration at 3 T with eight averages (*top* panel) and single average (*bottom* panel) after LCModel quantification. Acquisition times for eight-average data were 8.5, 4.25, 2.8 and 2.1 min, respectively; for single-average data, 64, 32, 21 and 16 s, respectively

one-dimensional SENSE acceleration can be utilized to accelerate the slow spatial phase encoding in a 2D PEPSI experiment. Further acceleration can be achieved using two-dimensional SENSE in 3D PEPSI experiments, where two orthogonal spatial phase encoding gradients are used. The SENSE PEPSI imaging technique presented can also be generalized to other echo-planar-based read-out methods, such as echo-shifted EPI (Guimaraes et al. 1999) or spiral (Adalsteinsson et al. 1998) MRSI. In those methods, oscillating read-out gradients are used to encode 2D spatial information in a single shot. In that regard, direct application of 2D SENSE would be

feasible. In fact, the cylindrically symmetric layout of the currently available head RF array coil encourages use of 2D SENSE to minimize the g-factor. As we noted earlier, in the future a large-*N* coil array may further increase the acceleration rate for high spatiotemporal resolution, with acceptable reconstructed spatiospectral MRSI data.

In conclusion, in this chapter, we presented the principle of parallel MRI with a brief review of recent advances in data acquisition and image reconstruction strategies. We also presented mathematical formulation of image reconstruction. We demonstrated examples of parallel MRI using SENSE reconstructions in EPI and brain fMRI to reduce geometrical distortion. In particular, we showed that with good prior knowledge about the image to be reconstructed, sensitivity-encoded echo-planer imaging (SENSE EPI) can be further stabilized to improve sensitivity and specificity in dynamic scanning. For spectroscopic imaging, we showed that MRSI experiments at high field (≥3T) may utilize parallel MRI to reduce imaging acquisition times with tolerable SNR reduction using single average PEPSI sequence, while low field (≤1.5T) may still use SENSE to reduce motion sensitivity and acquire multiple averages to maintain overall SNR. In conclusion, improvement of spatiotemporal resolution by parallel MRI can benefit static, dynamic, and metabolic MR imaging for cancer diagnosis and management.

Acknowledgements. We thank Dr. Stefan Posse and Dr. Larry Wald for their helpful comments. We also thank Nichole Eusemann for her help with the text. This work was supported by National Institutes of Health Grants R01 HD040712, R01 NS037462, P41 RR14075, R01 DA14178-01 and the Mental Illness and Neuroscience Discovery Institute (MIND).

REFERENCES

Adalsteinsson, E., Irarrazabal, P., Topp, S., Meyer, C., Macovski, A., and Spielman, D. M. (1998) Volumetric spectroscopic imaging with spiral-based k-space trajectories. *Magn. Reson. Med. 39*:889–898

Bammer, R., Keeling, S. L., Augustin, M., Pruessmann, K. P., Wolf, R., Stollberger, R., Hartung, H. P., and Fazekas, F. (2001) Improved diffusion-weighted single-shot echo-planar imaging (EPI) in stroke using sensitivity encoding (SENSE). *Magn. Reson. Med. 46*:548–554

Barth, M., Metzler, A., Klarhofer, M., Roll, S., Moser, E., and Leibfritz, D. (1999) Functional MRI of the human motor cortex using single-shot, multiple gradient-echo spiral imaging. *Magn. Reson. Imaging 17*:1239–1243

Beloueche-Babari, M., Jackson, L.E., Al-Saffar, N.M., Workman, P., Leach, M.O., and Ronen, S.M. (2005) Magnetic resonance spectroscopy monitoring of mitogen-activated protein kinase signaling inhibition. *Cancer Res. 65*:3356–3363

Breuer, F.A., Blaimer, M., Heidemann, R.M., Mueller, M.F., Griswold, M.A., and Jakob, P.M. (2005a) Controlled aliasing in parallel imaging results in higher acceleration (CAIPIRINHA) for multi-slice imaging. *Magn. Reson. Med. 53*:684–691

Breuer, F.A., Kellman, P., Griswold, M.A., and Jakob, P.M. (2005b) Dynamic autocalibrated parallel imaging using temporal GRAPPA (TGRAPPA). *Magn. Reson. Med. 53*:981–985

Brown, T.R., Kincaid, B.M., and Ugurbil, K. (1982) NMR chemical shift imaging in three dimensions. *Proc. Natl. Acad. Sci. USA 79*:3523–3526

Carlson, J.W., and Minemura, T. (1993) Imaging time reduction through multiple receiver coil data acquisition and image reconstruction. *Magn. Reson. Med. 29*:681–687

Dager, S.R., Friedman, S.D., Heide, A., Layton, M.E., Richards, T., Artru, A., Strauss, W., Hayes, C., and Posse, S. (1999) Two-dimensional

proton echo-planar spectroscopic imaging of brain metabolic changes during lactate-induced panic. *Arch. Gen. Psychiatry 56*:70–77

de Zwart, J.A., Ledden, P.J., Kellman, P., van Gelderen, P., and Duyn, J.H. (2002a) Design of a SENSE-optimized high-sensitivity MRI receive coil for brain imaging. *Magn. Reson. Med. 47*:1218–1227

de Zwart, J.A., van Gelderen, P., Kellman, P., and Duyn, J.H. (2002b) Application of sensitivity-encoded echo-planar imaging for blood oxygen level-dependent functional brain imaging. *Magn. Reson. Med. 48*:1011–1020

de Zwart, J.A., van Gelderen, P., Kellman, P., and Duyn, J.H. (2002c) Reduction of gradient acoustic noise in MRI using SENSE-EPI. *Neuroimage 16*:1151–1155

Del Sole, A., Falini, A., Ravasi, L., Ottobrini, L., De Marchis, D., Bombardieri, E., and Lucignani, G. (2001) Anatomical and biochemical investigation of primary brain tumours. *Eur. J. Nucl. Med 28*:1851–1872

Duyn, J.H., Gillen, J., Sobering, G., van Zijl, P.C., and Moonen, C.T. (1993) Multisection proton MR spectroscopic imaging of the brain. *Radiology 188*:277–282

Gillies, R.J., and Morse, D.L. (2005) In vivo magnetic resonance spectroscopy in cancer. *Annu. Rev. Biomed. Eng. 7*:287–326

Golay, X., Pruessmann, K.P., Weiger, M., Crelier, G.R., Folkers, P.J., Kollias, S.S., and Boesiger, P. (2000) PRESTO-SENSE: an ultrafast whole-brain fMRI technique. *Magn. Reson. Med. 43*:779–786

Golman, K., Ardenkjaer-Larsen, J.H., Petersson, J.S., Mansson, S., and Leunbach, I. (2003) Molecular imaging with endogenous substances. *Proc. Natl. Acad. Sci. USA 100*:10435–10439

Griswold, M.A., Jakob, P.M., Heidemann, R.M., Nittka, M., Jellus, V., Wang, J., Kiefer, B., and Haase, A. (2002) Generalized autocalibrating partially parallel acquisitions (GRAPPA). *Magn. Reson. Med. 47*:1202–1210

Guimaraes, A.R., Baker, J.R., Jenkins, B.G., Lee, P.L., Weisskoff, R.M., Rosen, B.R., and Gonzalez, R.G. (1999) Echoplanar chemical shift imaging. *Magn. Reson. Med. 41*:877–882

Haase, A. (1990) Snapshot FLASH MRI. Applications to T1, T2, and chemical-shift imaging. *Magn. Reson. Med. 13*:77–89

Haase, A., Frahm, J., Hanicke, W., and Matthaei, D. (1985) 1H NMR chemical shift selective (CHESS) imaging. *Phys. Med. Biol. 30*:341–344

Hansen, P.C. (1998) Rank-deficient and discrete ill-posed problems: numerical aspects of linear inversion. SIAM, Philadelphia, PA

Heberlein, K., and Hu, X. (2006) Auto-calibrated parallel spiral imaging. *Magn. Reson. Med. 55*:619–625

Hutchinson, M., and Raff, U. (1988) Fast MRI data acquisition using multiple detectors. *Magn. Reson. Med. 6*:87–91

Jakob, P.M., Griswold, M.A., Edelman, R.R., and Sodickson, D.K. (1998) AUTO-SMASH: a self-calibrating technique for SMASH imaging. Simultaneous acquisition of spatial harmonics. *Magma 7*:42–54

Kellman, P., Epstein, F.H., and McVeigh, E.R. (2001) Adaptive sensitivity encoding incorporating temporal filtering (TSENSE). *Magn. Reson. Med. 45*:846–852

Kuhn, B., Dreher, W., Norris, D.G., and Leibfritz, D. (1996) Fast proton spectroscopic imaging employing k-space weighting achieved by variable repetition times. *Magn. Reson. Med. 35*:457–464

Lin, F.H., Chen, Y.J., Belliveau, J.W., and Wald, L.L. (2003) A wavelet-based approximation of surface coil sensitivity profiles for correction of image intensity inhomogeneity and parallel imaging reconstruction. *Hum. Brain Mapp. 19*:96–111

Lin, F.H., Kwong, K.K., Belliveau, J.W., and Wald, L.L. (2004) Parallel imaging reconstruction using automatic regularization. *Magn. Reson. Med. 51*:559–567

Lin, F.H., Huang, T.Y., Chen, N.K., Wang, F.N., Stufflebeam, S.M., Belliveau, J.W., Wald, L.L., and Kwong, K.K. (2005) Functional MRI using regularized parallel imaging acquisition. *Magn. Reson. Med. 54*:343–353

Madore, B. (2004) UNFOLD-SENSE: a parallel MRI method with self-calibration and artifact suppression. *Magn. Reson. Med. 52*:310–320

Madore, B., Glover, G.H., and Pelc, N.J. (1999) Unaliasing by fourier-encoding the overlaps using the temporal dimension (UNFOLD), applied to cardiac imaging and fMRI. *Magn. Reson. Med. 42*:813–828

Maudsley, A.A., Matson, G.B., Hugg, J.W., and Weiner, M.W. (1994) Reduced phase encoding in spectroscopic imaging. *Magn. Reson. Med. 31*:645–651

McKenzie, C.A., Ohliger, M.A., Yeh, E.N., Price, M.D., and Sodickson, D.K. (2001) Coil-by-coil image reconstruction with SMASH. *Magn. Reson. Med. 46*:619–623

McKinnon, G.C. (1993) Ultrafast interleaved gradient-echo-planar imaging on a standard scanner. *Magn. Reson. Med. 30*:609–616

O'Sullivan, J. (1985) A fast sinc function gridding algorithm for Fourier inversion in computer tomography. *IEEE Trans. Med. Imaging MI-4*:200–207

Pohmann, R., von Kienlin, M., and Haase, A. (1997) Theoretical evaluation and comparison of fast chemical shift imaging methods. *J. Magn. Reson. 129*:145–160

Posse, S., DeCarli, C., and Le Bihan, D. (1994) Three-dimensional echo-planar MR spectroscopic imaging at short echo times in the human brain. *Radiology 192*:733–738

Posse, S., Tedeschi, G., Risinger, R., Ogg, R., and Le Bihan, D. (1995) High speed 1H spectroscopic imaging in human brain by echo planar spatial-spectral encoding. *Magn. Reson. Med. 33*:34–40

Posse, S., Dager, S.R., Richards, T.L., Yuan, C., Ogg, R., Artru, A.A., Muller-Gartner, H. W., and Hayes, C. (1997) In vivo measurement of regional brain metabolic response to hyperventilation using magnetic resonance: proton echo planar spectroscopic imaging (PEPSI). *Magn. Reson. Med. 37*:858–865

Preibisch, C., Pilatus, U., Bunke, J., Hoogenraad, F., Zanella, F., and Lanfermann, H. (2003) Functional MRI using sensitivity-encoded echo planar imaging (SENSE-EPI). *Neuroimage 19*:412–421

Preul, M.C., Caramanos, Z., Collins, D.L., Villemure, J.G., Leblanc, R., Olivier, A., Pokrupa, R., and Arnold, D.L. (1996) Accurate, noninvasive diagnosis of human brain tumors by using proton magnetic resonance spectroscopy. *Nat. Med. 2*:323–325

Preul, M.C., Caramanos, Z., Leblanc, R., Villemure, J.G., and Arnold, D.L. (1998) Using pattern analysis of in vivo proton MRSI data to improve the diagnosis and surgical management of patients with brain tumors. *NMR Biomed. 11*:192–200

Pruessmann, K.P., Weiger, M., Scheidegger, M.B., and Boesiger, P. (1999) SENSE: sensitivity encoding for fast MRI. *Magn. Reson. Med. 42*: 952–962

Pruessmann, K.P., Weiger, M., Bornert, P., and Boesiger, P. (2001) Advances in sensitivity encoding with arbitrary k-space trajectories. *Magn. Reson. Med. 46*:638–651

Ra, J.B., and Rim, C.Y. (1993) Fast imaging using subencoding data sets from multiple detectors. *Magn. Reson. Med. 30*:142–145

Roemer, P.B., Edelstein, W.A., Hayes, C.E., Souza, S.P., and Mueller, O.M. (1990) The NMR phased array. *Magn. Reson. Med. 16*:192–225

Schmidt, C.F., Degonda, N., Luechinger, R., Henke, K., and Boesiger, P. (2005) Sensitivity-encoded (SENSE) echo planar fMRI at 3T in the medial temporal lobe. *Neuroimage 25*:625–641

Sodickson, D.K. (2000) Tailored SMASH image reconstructions for robust in vivo parallel MR imaging. *Magn. Reson. Med. 44*:243–251

Sodickson, D.K., and Manning, W.J. (1997) Simultaneous acquisition of spatial harmonics (SMASH): fast imaging with radiofrequency coil arrays. *Magn. Reson. Med. 38*:591–603

Sodickson, D.K., and McKenzie, C.A. (2001) A generalized approach to parallel magnetic resonance imaging. *Med. Phys. 28*:1629–1643

Tikhonov, A.N., and Arsenin, V.I. (1977) Solutions of ill-posed problems. Winston, Washington, DC and New York; distributed solely by Halsted Press

Tsao, J., Boesiger, P., and Pruessmann, K.P. (2003) k-t BLAST and k-t SENSE: dynamic MRI with high frame rate exploiting spatiotemporal correlations. *Magn. Reson. Med. 50*:1031–1042

Weiger, M., Pruessmann, K.P., Kassner, A., Roditi, G., Lawton, T., Reid, A., and Boesiger, P. (2000) Contrast-enhanced 3D MRA using SENSE. *J. Magn. Reson. Imaging 12*:671–677

Weiger, M., Pruessmann, K.P., and Boesiger, P. (2002a) 2D SENSE for faster 3D MRI. *Magma 14*:10–19

Weiger, M., Pruessmann, K.P., Osterbauer, R., Bornert, P., Boesiger, P., and Jezzard, P. (2002b) Sensitivity-encoded single-shot spiral imaging for reduced susceptibility artifacts in BOLD fMRI. *Magn. Reson. Med. 48*:860–866

Yeh, E.N., McKenzie, C.A., Ohliger, M.A., and Sodickson, D.K. (2005a) Parallel magnetic

resonance imaging with adaptive radius in k-space (PARS): constrained image reconstruction using k-space locality in radiofrequency coil encoded data. *Magn. Reson. Med. 53*:1383–1392

Yeh, E.N., Stuber, M., McKenzie, C.A., Botnar, R.M., Leiner, T., Ohliger, M.A., Grant, A.K., Willig-Onwuachi, J.D., and Sodickson, D.K. (2005b) Inherently self-calibrating non-Cartesian parallel imaging. *Magn. Reson. Med. 54*:1–8